

www.acsanm.org Article

Plasmon-Enhanced Photocatalytic Oxidation of Benzyl Alcohol to Benzaldehyde Using BiVO₄/BiOBr/Au Nanosheets

Ahmed E. ElMetwally, Mostafa Saad Sayed, Jae-Jin Shim, Marc R. Knecht, and Leonidas G. Bachas*



Cite This: ACS Appl. Nano Mater. 2023, 6, 5909–5917



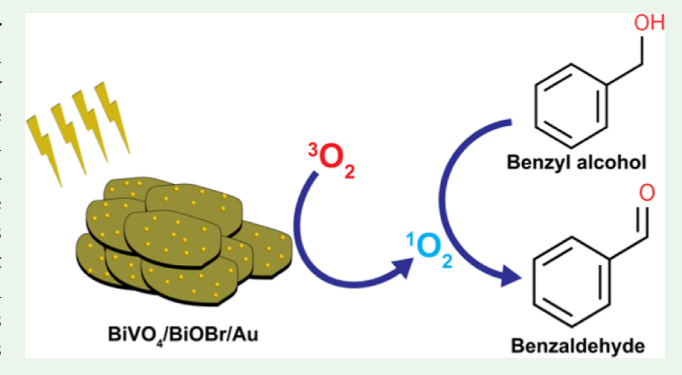
ACCESS

III Metrics & More

Article Recommendations

Supporting Information

ABSTRACT: Plasmonic Au nanoparticles were deposited over photocatalytic BiVO₄/BiOBr nanosheets with different loadings in the range of 0.5–5% (w/w) to boost the photocatalytic reactivity via surface plasmonic resonance. The results showed that the highest benzyl alcohol conversion (100%) and the maximum benzaldehyde yield (99%) were obtained using BiVO₄/BiOBr/Au 3% after 4 h of irradiation. Electron paramagnetic resonance analysis and trapping experiments revealed that singlet oxygen is the dominant species produced within the system and suggest that it is the main species driving photocatalytic oxidation of benzyl alcohol to benzaldehyde. The proposed mechanism involves irradiation of BiVO₄/BiOBr/Au with light to excite its electrons to the singlet state and produce singlet excitons, which eventually



produces triplet excitons via intersystem crossing. Dissolved O₂ subsequently reacts with these triplet excitons to produce singlet oxygen. Moreover, the energy barrier and the intrinsic reaction indicated that the reaction is thermodynamically favorable. These results demonstrate the unique effects of plasmonic resonance on photocatalytic activity, which can be adapted to different selective oxidation reactions.

KEYWORDS: surface plasmon, nanoparticles, photocatalysis, oxidation, benzaldehyde

■ INTRODUCTION

Eclectic oxidation of aromatic alcohols to their corresponding aldehydes has attracted great attention as it is a fundamental organic transformation that provides critical insight into both basic and practical research processes. 1,2 Among these aldehydes, benzaldehyde is primarily used by the chemical industry for the synthesis of various organic compounds including flavorings, food additives, perfumes, aniline dyes, and pharmaceuticals.^{3–5} Typically, the production of benzaldehyde takes place via benzyl chloride hydrolysis, toluene oxidation, or benzyl alcohol oxidation. However, these procedures suffer from different shortcomings including the generation of toxic byproducts, high starting material costs, and use of harmful oxidants. 6-9 Thus, the development of a greener sustainable pathway to eclectically oxidize aromatic alcohols to their corresponding aldehydes is necessary to meet the ambitions for green and sustainable production of chemicals.

Solar energy has been introduced as a clean sustainable energy source that can efficiently drive chemical reactions. ^{10–19} Recently, researchers have expressed interest in photocatalytic selective oxidation reactions because of their promising potential for driving organic transformations. For this reason, different photocatalysts have been explored such as g-C₃N₄, TiO₂, CdS, WO₃, Bi₂WO₆, Bi₂MoO₆, and MoS₂ to enhance the photocatalytic partial oxidation of benzyl alcohol to benzalde-

hyde.^{20–24} Unfortunately, these systems still suffer from low performance and poor selectivity toward benzaldehyde. To overcome these shortcomings, a photocatalyst must be carefully designed by considering certain aspects including the valence band and conduction band potentials to avoid the production of certain reactive oxygen species, such as hydroxyl radicals, that might lead to the overoxidation or breakdown of benzaldehyde.²⁵ In addition, a highly efficient photocatalyst should ideally be fully functional and able to produce photogenerated charge carriers in visible light, as this accounts for half of the sun's total energy. Furthermore, the photocatalyst ideally should be capable of interacting with reactant molecules via adsorption, electrostatic interaction, or bonding to obtain the maximum performance.⁶

To achieve these requirements, bismuth vanadate ($BiVO_4$) has been introduced as a promising visible-light-active photocatalyst with robust potential for selective oxidation reactions. ²⁶ $BiVO_4$ is an n-type semiconductor with a band gap

Received: January 19, 2023 Accepted: March 21, 2023 Published: March 30, 2023





in the range of 2.5-2.6 eV, which allows it to generate charge carriers upon irradiation with visible light.²⁷ In addition, the valence band alignment of BiVO₄ allows it to produce photogenerated holes, while its conduction band alignment is not negative enough to drive reduction reactions.²⁶ Despite its outstanding photocatalytic activity, the fast recombination of the photogenerated charge carriers significantly affects its apparent quantum efficiency.²⁸ Thus, designing a heterojunction that comprises BiVO₄ as an n-type semiconductor and another p-type semiconductor is necessary to reduce the recombination rate of the photogenerated charge carriers.²⁹ BiOX (X = Cl, Br, or I) is a Bi-based semiconductor that has been extensively used as a photocatalyst because of its excellent photocatalytic activity. On these accounts, in the present study, BiOBr was selected because its band gap matches that of BiVO₄ to form a type II p-n heterojunction.³

The deposition of plasmonic nanodomains can foster the photocatalytic performance of $\rm BiVO_4/BiOBr$ nanosheets by inducing a surface plasmonic resonance (SPR) effect. This effect occurs as a result of the rapid oscillations of the excited electrons throughout the nanodomains upon irradiation of these components with a specific wavelength of light, which leads to the formation of a Schottky junction. This junction promotes the electron/hole separation and expands the absorption capacity of the photocatalyst.

Furthermore, plasmonic nanodomains create a dielectric polarization effect that significantly fosters the reactant adsorption on the surface of the catalyst, which in turn decreases mass-transfer limitations.³⁴ On these accounts, it is likely that the decoration of BiVO₄/BiOBr with Au nanodomains could enhance the photocatalytic performance of BiVO₄/BiOBr toward the selective oxidation of benzyl alcohol to benzaldehyde.

Herein, an efficient strategy has been introduced for the preparation of BiVO₄/BiOBr decorated with Au nanodomains to enhance the photocatalytic selective oxidation of benzyl alcohol to benzaldehyde. In particular, BiVO₄/BiOBr was prepared using a one-pot synthesis method, followed by photodeposition of the Au nanodomains. After comprehensive characterization, the materials were examined in the photocatalytic selective oxidation of benzyl alcohol to benzaldehyde. The data showed a substantial improvement in the photocatalytic performance compared to bare BiVO₄/BiOBr. Moreover, the oxidation pathway of benzyl alcohol to benzaldehyde was examined, where a mechanism of singlet oxygen generation is suggested that leads to the selective generation of the final product.

EXPERIMENTAL SECTION

Materials. Bismuth(III) nitrate pentahydrate, hydrogen tetrachloroaurate(III) trihydrate (Au 49%), and ammonium metavanadate were obtained from Alfa Aesar. Cetyltrimethylammonium bromide (CTAB), benzyl alcohol, benzaldehyde, and p-anisaldehyde were purchased from Sigma-Aldrich. Methanol was supplied by VWR. All compounds were used as received. Ultrapure deionized water (18.1 M Ω cm) was used for all experiments in this study, unless mentioned otherwise.

Preparation of BiVO₄/**BiOBr.** To prepare $BiVO_4/BiOBr$, 970 mg of bismuth(III) nitrate pentahydrate was dissolved in 10 mL of deionized water at room temperature until a whitish slurry was formed. Then, 117 mg of ammonium metavanadate was dissolved in 10 mL of deionized water at 90 $^{\circ}$ C; once dissolved, the ammonium metavanadate solution was cooled down to room temperature. Next, a three-neck round bottom flask outfitted with a condenser was

immersed in an oil bath at 60 °C to which 365 mg of CTAB was added to 20 mL of water under stirring. Subsequently, the oil bath temperature was raised to 80 °C, followed by the dropwise addition of the ammonium metavanadate solution and finally the dropwise addition of the bismuth(III) nitrate pentahydrate whitish slurry to obtain a yellowish slurry. The mixture was kept under stirring for 16 h at 80 °C. Eventually, the canary yellowish precipitate was filtered and washed with deionized water, followed by ethanol, and dried in vacuo at 60 °C overnight.

Preparation of BiVO₄/BiOBr/Au. To prepare BiVO₄/BiOBr/Au, a borosilicate glass vial (60 mL) with a silicone septum cap was charged with 200 mg of BiVO₄/BiOBr material, and then deionized water (50 mL) was added, followed by sonication for 10 min. Select amounts of hydrogen tetrachloroaurate(III) trihydrate were dissolved in deionized water to obtain different Au loadings of 0.5, 1, 3, and 5% (w/w), where the Au solution was added to the BiVO₄/BiOBr slurry. Next, 1 mL of methanol was added as a hole scavenger; the borosilicate glass vial was carefully sealed, and the vial was purged with nitrogen for 30 min prior to irradiation with light. To initiate a photodeposition reaction, the borosilicate glass vial was irradiated using an Oriel Instruments solar simulator that is equipped with a 300 W high-power mercury-xenon lamp for 45 min. Eventually, a greenish yellow precipitate was formed, filtered, and rinsed with deionized water, followed by ethanol, and dried in vacuo at 60 °C overnight.

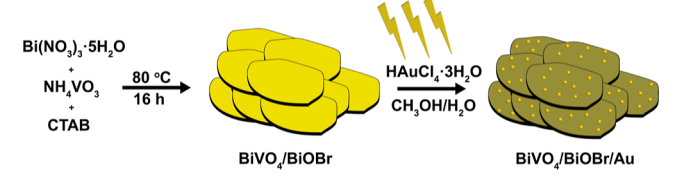
Characterization. A JEOL JEM-1400 microscope operating at 80 kV was used to obtain the transmission electron microscopy (TEM) images, while an FEI F200i transmission electron microscope operating at 200 kV was used to obtain the high-resolution TEM (HRTEM) images, energy-dispersive X-ray spectroscopy (EDS), and line scan profile analyses. The SEM images were obtained using a JEOL 7100F SEM system operating at 30 kV. A Panalytical X'Pert PRO MPD X-ray diffractometer was used for X-ray diffraction (XRD) analysis using Cu K α radiation (1.54 Å). Diffuse reflectance spectroscopy (DRS) analysis was conducted on a Shimadzu model UV-2600 system. Finally, the elemental content within the samples was identified using an Agilent 720 inductively coupled plasmaoptical emission spectroscopy (ICP-OES) spectrometer. A Micromeritics 3Flex surface characterization analyzer was used for N₂ adsorption-desorption analysis at -196 °C. Before the measurements, the materials were outgassed at 120 °C for 10 h.

Selective Oxidation of Benzyl Alcohol to Benzaldehyde. For each experiment, a borosilicate glass vial (40 mL) was charged with 30 mg of the photocatalyst and 30 mL of benzyl alcohol (500 μ M in 50:50 (v/v) acetonitrile/water). The mixture was sonicated for 30 s in an ultrasonic bath (Branson M2800) and stirred in the dark to achieve adsorption-desorption equilibrium. Next, the vial was placed in an Ace Glass photochemical safety cabinet, model #7836-20, that is equipped with a 450 W medium-pressure mercury-vapor lamp. At preset intervals, 500 μ L aliquots were withdrawn and transferred to 2 mL gas chromatography (GC) vials, to which 500 μ L of GC-grade hexane was added. To extract the reactant and products into the hexane layer, the vials were agitated on a vortexer for 1 h. Then, aliquots (100 μ L) were withdrawn from the hexane layer and transferred to a 1.8 mL GC vial with a 200 μ L glass insert, to which 10 μL of p-anisaldehyde was spiked as an internal standard. All samples were analyzed on an Agilent GC-MS 5975C equipped with a HP-5MS column with a length of 30 m, an ID of 0.250 mm, and a film thickness of 0.25 μ m.

■ RESULTS AND DISCUSSION

BiVO₄/BiOBr was prepared and decorated with Au nanodomains. The procedure used involves a simple green approach to prepare a highly efficient multicomponent photocatalyst. Interestingly, this approach involves the use of a one-pot method to prepare BiVO₄/BiOBr, which enables the intercalation between BiOBr and BiVO₄. Moreover, it describes a green route to deposit Au nanoparticles using a simple photodeposition approach, as shown in Scheme 1.

Scheme 1. Preparation of BiVO₄/BiOBr/Au



The structure of the prepared BiVO₄/BiOBr photocatalyst before and after Au loadings was examined using XRD analysis, where the obtained patterns are presented in Figure 1a. The XRD pattern of BiVO₄/BiOBr shows peaks at 18.7, 28.8, 30.5, 35.2, 39.8, 42.5, 47.3, 50.3, 53.3, and 58.5° that correspond to the (110), (121), (040), (002), (211), (051), (042), (202), (161), and (321) planes of BiVO₄. The pattern of BiVO₄ can be indexed to the monoclinic phase of BiVO₄ (JCPDS no. 00-014-0688),³⁵ as displayed in the Supporting Information, Figure S1. On the other hand, the peaks appearing at 10.9, 25.3, 31.9, 39.3, 46.5, and 57.2° correspond to the (001), (101), (102), (112), (200), and (203) planes of BiOBr. The pattern of BiOBr can be indexed to the tetragonal phase of BiOBr (JCPDS no. 00-001-1004),³⁶ as displayed in Supporting Information, Figure S1. To obtain insights on how the photodeposition of Au nanoparticles could influence the photocatalytic reactivity toward benzyl alcohol oxidation, Au nanodomains were deposited on BiVO₄/BiOBr with different loadings in the range of 0.5-5 wt %. The patterns of the BiVO₄/BiOBr/Au samples show an additional peak at 38.2° that corresponds to the (111) plane of cubic gold nanoparticles (Figure 1a) according to JCPDS no. 00-001-1172 (Supporting Information, Figure S1).³⁷ The intensity of the Au peaks increases with increasing gold content; however, the Au peaks in the 0.5% sample can be barely seen because the gold content is too low to be detected via XRD analysis. Moreover, there are no peaks observed for gold oxide nanoparticles indicating that

all the gold particles formed on the surface of ${\rm BiVO_4/BiOBr}$ are Au nanodomains.

SEM analysis was conducted to investigate thoroughly the effect of photodeposition on the morphology of BiVO₄/BiOBr, and the obtained images are presented in Figure 1c,d. The SEM image of the prepared bare BiVO₄/BiOBr (Figure 1c) reveals that the nanomaterial has a sheet-like structure with a smooth surface, where each nanosheet was stacked on top of one another. After 3% Au photodeposition, small particles were formed on the BiVO₄/BiOBr nanosheets that correspond to Au nanoparticles (Figure 1d). Particularly, and to ensure that Au nanodomains are formed on the BiVO₄/BiOBr nanosheets, the bare BiVO₄/BiOBr particles were ultrasonically dispersed in water, and the gold precursor solution was added to the dispersed nanosheet slurry and stirred for 30 min prior to the photodeposition reaction. During this 30 min period, the gold ions were adsorbed on the BiVO₄/BiOBr nanosheet surface; thus, when Au nanodomains were grown, they were deposited on the nanosheet surface. In addition, the SEM image of BiVO₄/BiOBr/Au 3% demonstrates that the nanosheets structure remains intact during and after photodeposition.

The effect of Au loadings on the morphology of BiVO₄/BiOBr nanosheets was also studied using TEM analysis, and the images are displayed in Figure S2. The TEM images of BiVO₄/BiOBr/Au samples exhibit small dark particles that are unevenly dispersed over the nanosheets. Interestingly, the number of these dark particles did not increase with increasing the Au loading, but instead the size of the deposited particles increased with increasing the Au loading. This phenomenon indicates that upon increasing the Au precursor concentration, Au ions are reduced to make the existing particles larger rather than forming new particles. The Au content within the BiVO₄/BiOBr/Au samples was also analyzed using ICP–OES, and the obtained data are listed in Table S1.

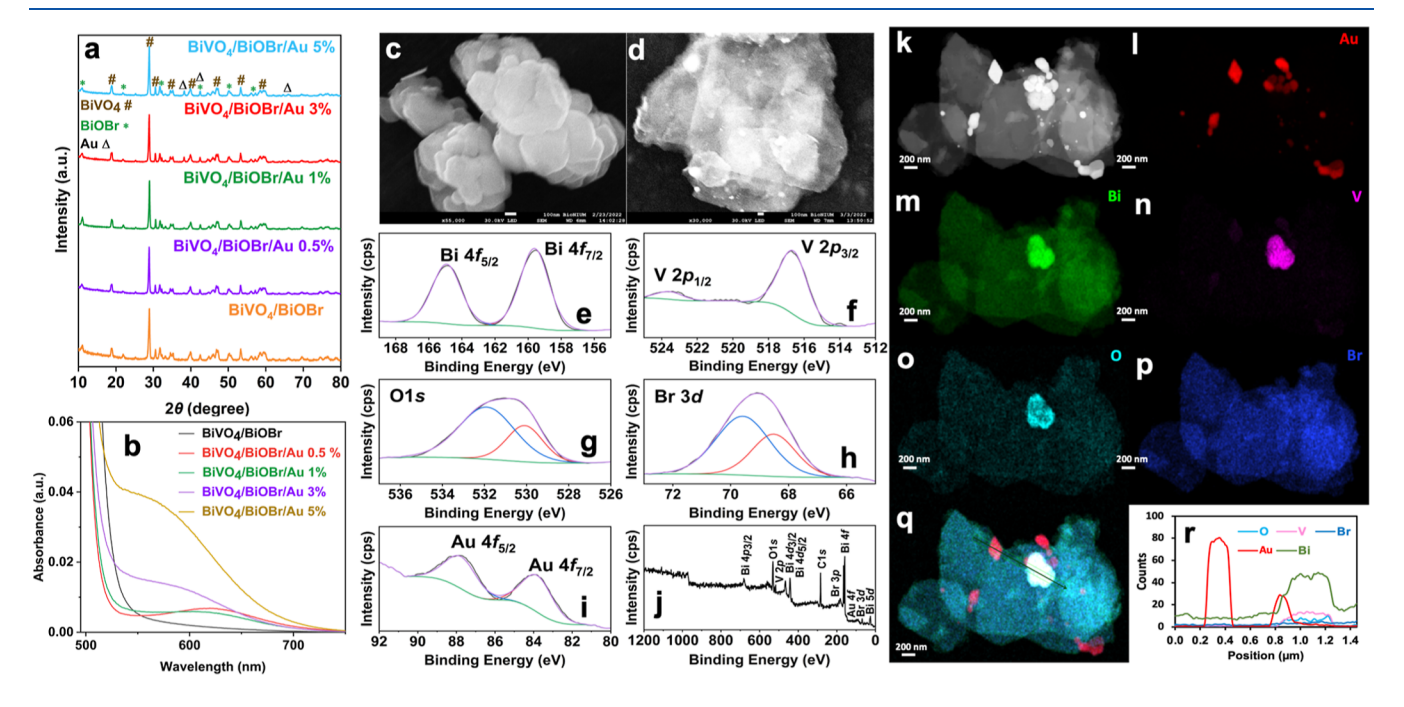


Figure 1. (a) XRD patterns; (b) UV-vis spectra of BiVO₄/BiOBr and BiVO₄/BiOBr/Au with different loadings; SEM images of (c) BiVO₄/BiOBr and (d) BiVO₄/BiOBr/Au 3%; high-resolution XPS spectra of (e) Bi 4f, (f) V 2p, (g) O 1s, (h) Br 3d, and (i) Au 4f; (j) wide spectrum, (k) HRTEM image, (l-q) EDS mapping, and (r) line-scan profile of BiVO₄/BiOBr/Au 3%.

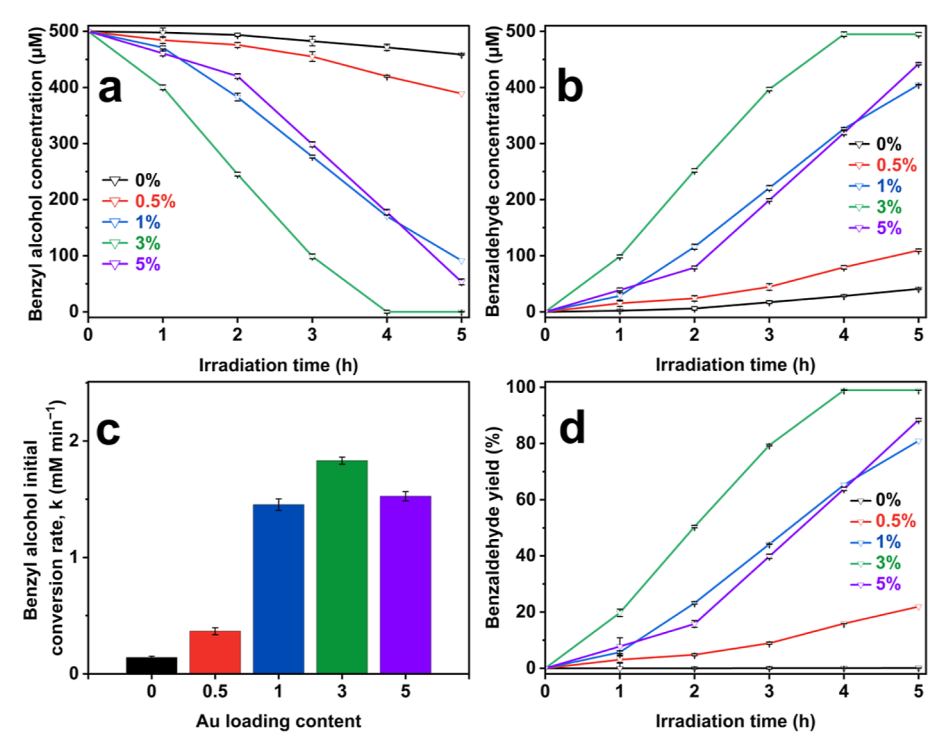


Figure 2. Photocatalytic oxidation of benzyl alcohol: (a) benzyl alcohol disappearance, (b) benzaldehyde appearance, (c) initial conversion rate of benzyl alcohol, and (d) benzaldehyde yield. Conditions: benzyl alcohol concentration (500 μ M), pH (6.8), photocatalyst weight (30 mg), and temperature (20 °C). Percent of Au on BiVO₄/BiOBr/Au ranges from 0 to 5%.

The surface chemical state of the nanosheets of BiVO₄/ BiOBr was further explored using X-ray photoelectron spectroscopy (XPS) analysis, and the obtained spectra are presented in the Supporting Information, Figure S3. The Bi 4f spectrum of BiVO₄/BiOBr shows two peaks at 159.5 and 165 eV, which correspond to the binding energies of Bi 4f_{7/2} and Bi $4f_{5/2}$ respectively. These values agree well with the Bi³⁺ values reported for BiOBr elsewhere.³⁸ The V 2p spectrum exhibits two peaks at 516.5 and 524 eV that are assigned to $V 2p_{3/2}$ and V $2p_{1/2}$, respectively, which were attributed to V^{5+} of monoclinic BiVO₄.³⁹ The O 1s spectrum shows two peaks at 529.5 and 531.5 eV, arising from the lattice oxygen of tetragonal BiOBr and monoclinic BiVO₄. 38 Separately, the peaks for Br $3d_{3/2}$ and Br $3d_{5/2}$ appear at 69.5 and 68.2 eV, respectively, arising from the bromide ions of tetragonal BiOBr.³⁹ After the photodeposition of Au nanoparticles, the XPS spectra of BiVO₄/BiOBr/Au 3% exhibit all the major peaks of Bi, V, O, and Br without any noticeable shift in their binding energies, as shown in Figure 1e-j. The two peaks at 83.9 and 87.7 eV (Figure 1i) correspond to Au $4f_{7/2}$ and Au $4f_{5/2}$, respectively, and can be indexed to metallic Au.

To explore the distribution of the elements across the nanosheets of BiVO₄/BiOBr/Au, HRTEM and elemental mapping analyses were carried out (Figure 1k-q). The results reveal that bismuth, oxygen, and bromine are homogeneously distributed across the BiOBr sheet, while vanadium intensifies within the BiVO₄ sheet. In addition, the elemental mapping of BiVO₄/BiOBr/Au reveals that gold nanodomains were deposited on both BiOBr and BiVO₄ nanosheets. These results were further investigated by line-scan profile analysis (Figure 1r), which reveals that vanadium was only found at the BiVO₄ sheet, while bismuth was detected at both BiOBr and BiVO₄ sheets. In addition, the gold profile shows that Au nanodomains were formed on both BiOBr and BiVO₄.

DRS analysis was conducted to estimate the band edge positions of the prepared materials, and the obtained spectra are shown in Supporting Information, Figure S4. It is evident that there was no significant shift in the absorption edge positions or the band gaps of the prepared materials after the deposition of metallic gold nanoparticles. On the other hand, UV—vis spectra (Figure 1b) show an additional shoulder peak in the visible region that corresponds to the surface plasmon of metallic gold nanoparticles. Moreover, it was evident that the intensity of this peak increases and becomes blue-shifted with increasing the Au content in the sample. The blue-shifted surface plasmon is due to the long-range dipole coupling in the gold nanoparticle random arrays. 41

The surface area of the BiVO₄/BiOBr materials before and after gold deposition was quantified using $\rm N_2$ adsorption—desorption analysis, and the generated isotherms are presented in Figure S5. It is evident that the materials before and after gold deposition exhibit reversible type II isotherms, and this type of isotherm is encountered when $\rm N_2$ adsorption—desorption occurs on non-porous materials. The SEM analysis also confirms the non-porous texture of the prepared materials. The BET surface area calculated for the BiVO₄/BiOBr materials before and after gold deposition was found to be 1.73 and 2.04 m²/g for BiVO₄/BiOBr and BiVO₄/BiOBr/Au 3%, respectively. It is evident that the surface area increased upon the deposition of gold, which can be ascribed to the additional surface area provided by the surface of the gold nanoparticles.

Once the prepared BiVO₄/BiOBr/Au samples with different loadings of Au were comprehensively characterized, their reactivity was tested in the photocatalytic oxidation of benzyl alcohol to benzaldehyde in a photochemical reactor. Prior to photocatalytic experiments, the adsorption capacity of the BiVO₄/BiOBr/Au samples was examined, and the results are

presented in the Supporting Information, Figure S6. The data revealed that negligible benzyl alcohol adsorption occurred, which did not exceed 0.25% for all the tested samples. Furthermore, it was evident that 30 min of stirring was adequate for all the tested materials to equilibrate with benzyl alcohol. As such, all the tested photocatalysts were stirred for 30 min in the dark before initiating the reaction to attain adsorption—desorption equilibrium.

Before evaluating the reactivity of the prepared BiVO₄/BiOBr/Au nanomaterials for photocatalysis, the reaction was conducted in absence of the prepared nanomaterials (Supporting Information, Figure S7). The results show that after 5 h of irradiation, the extent of benzyl alcohol conversion did not exceed 1%, revealing that light alone, without a photocatalyst, cannot drive the oxidation of benzyl alcohol to benzaldehyde. In addition, there were no detectable products observed during the irradiation of benzyl alcohol in the absence of a photocatalyst, emphasizing the importance of using an efficient photocatalyst to drive the reaction.

The photocatalytic oxidation of benzyl alcohol was initiated by irradiating the sample once the photocatalyst had equilibrated with benzyl alcohol. The concentrations of benzyl alcohol and benzaldehyde were monitored as a function of time, as shown in Figure 2. The results revealed that the extent of benzyl alcohol conversion was quite sluggish in the presence of Au-free BiVO₄/BiOBr. Upon testing the BiVO₄/BiOBr/Au samples, the extent of benzyl alcohol conversion significantly increased. The results showed that the extent of benzyl alcohol conversion and benzaldehyde yield increased with increasing the Au content, reaching maximum reactivity when the Au content was 3%. Beyond this loading, the reactivity declined.

The observed reactivity enhancement was attributed to the surface plasmon resonance (SPR) and arises upon promoting the BiVO₄/BiOBr material with plasmonic nanoparticles such as Au nanoparticles. The SPR can be readily activated upon irradiation with light that excites the collective electrons of the plasmonic nanoparticles. Accordingly, surface plasmons are formed as a result of a rapid oscillation of the electrons at metallic-dielectric interfaces. 42 Such an improvement expands the light absorption capacity of the semiconducting material to harness the visible light irradiation, which eventually fosters the photocatalytic performance.³² In addition, when a semiconductor is promoted with plasmonic nanoparticles, a Schottky junction is created, generating an electric field that enhances the separation of the charge carriers, increasing their formation rate while restraining their recombination.³⁴ Furthermore, surface plasmons are capable of polarizing the reactants at the metal/liquid interface owing to the dielectric polarization effect, thus reducing the mass transport limitation at the photocatalyst surface.³³ A maximum benzaldehyde yield of 99% was obtained using BiVO₄/BiOBr/Au 3%; beyond an Au content of 3%, the benzaldehyde yield declined. This decline occurred because the gold particles tend to grow in size rather than form new particles, as shown in the TEM images. The formation of large Au nanoparticles limits their exposure to light irradiation and reduces their photocatalytic performance.

The feasibility of the prepared composite was further evaluated by comparing the photocatalytic activity of $BiVO_4/BiOBr/Au$ 3% with that of $BiVO_4/Au$ 3% and BiOBr/Au 3%, and the obtained data are presented in Figure S8. The data revealed that the maximum efficiency was obtained when using $BiVO_4/BiOBr/Au$ 3%, indicating the crucial role of the

composite in enhancing the photocatalytic performance. To estimate the conduction and valence band edge positions of the composite, Mott-Schottky, DRS, and valence band XPS analyses were conducted. The DRS data show (Supporting Information, Figure S9a,b) that BiVO₄ and BiOBr have a band gap of 2.6 and 2.9 eV, respectively. In addition, the valence band XPS curves of BiVO₄ and BiOBr (Supporting Information, Figure S9c,d) were used to obtain the value of energy gap between the VB and the Fermi level (E_f) . For the BiVO₄, this gap was found to be 2.1 eV, while that for BiOBr was found to be 1.7 eV. Mott-Schottky analysis was used to obtain the value of the Fermi level (E_f) for both BiVO₄ and BiOBr, as shown in Supporting Information, Figure S9e. The results revealed that $BiVO_4$ and BiOBr have Fermi level (E_f) values of -0.37 and -0.32, respectively. Interestingly, the Mott-Schottky plots of BiVO₄ and BiOBr exhibit a positive slope which is encountered with n-type semiconductors. Accordingly, the conduction bands (Supporting Information, Figure S9f) for BiVO₄ and BiOBr were calculated, and their values were found to be -0.62 and -1.53 eV, respectively.

The performance of BiVO₄/BiOBr/Au 3% in the photocatalytic oxidation of benzyl alcohol to benzaldehyde (substrate conversion of 100% and benzaldehyde selectivity of 99%) after 4 h of irradiation is noteworthy, especially when compared with other photocatalysts that have been used previously for this reaction. For example, Schünemann et al. 43 prepared a composite made up of halide perovskites and titanium oxide, where they tested the prepared composite for this reaction. They reported that the composite was able to have a benzyl alcohol to benzaldehyde conversion of 50% and benzaldehyde selectivity of 99% after 20 h of irradiation. Shen et al.44 prepared ultrathin nanosheets of Bi₄Ti₃O₁₂ and examined the photocatalytic activity of the nanosheets. For these materials, it was found that after 5 h of irradiation, the conversion of benzyl alcohol reached 35.5%, while the benzaldehyde selectivity was 99.8%. Alternatively, Zou et al. 45 synthesized ZnTi-LDH nanosheets as photocatalysts, where they reported a benzyl alcohol conversion of 61% and a benzaldehyde selectivity of 77% after 4 h of irradiation. Xing et al. 46 prepared a polyoxometalate-incorporated ZnIn₂S₄ Zscheme dual-functional photocatalyst for the selective oxidation of benzyl alcohol to benzaldehyde. The prepared photocatalyst exhibited a photocatalytic activity with benzyl alcohol conversion and benzaldehyde selectivity of 96.1 and 98.2%, respectively, after 25 h of irradiation. Giannakoudakis et al.47 prepared nanostructured titanium (hydro)oxide and tested the photocatalytic activity of the prepared titanium (hydro)oxide in benzyl alcohol oxidation. They reported a benzyl alcohol conversion of 73% and a benzaldehyde selectivity of almost 100% after 6 h of UV irradiation. Thus, it is evident that BiVO₄/BiOBr/Au 3% exhibited enhanced photocatalytic performance compared to previous systems. Moreover, the GC-MS chromatograms (Supporting Information, Figures S10,S11) show that benzaldehyde is the only oxidative product generated over the course of the reaction. In addition, no intermediates were detected during the reaction, indicating that benzyl alcohol is directly oxidized to benzaldehyde.

To get insights on the reactive oxygen species that might drive the photocatalytic oxidation process, trapping experiments were conducted by adding a selective trap for each reactive oxygen species. For such experiments, *p*-benzoquinone (BQ), isopropanol (IPA), triethanolamine (TEOA), and

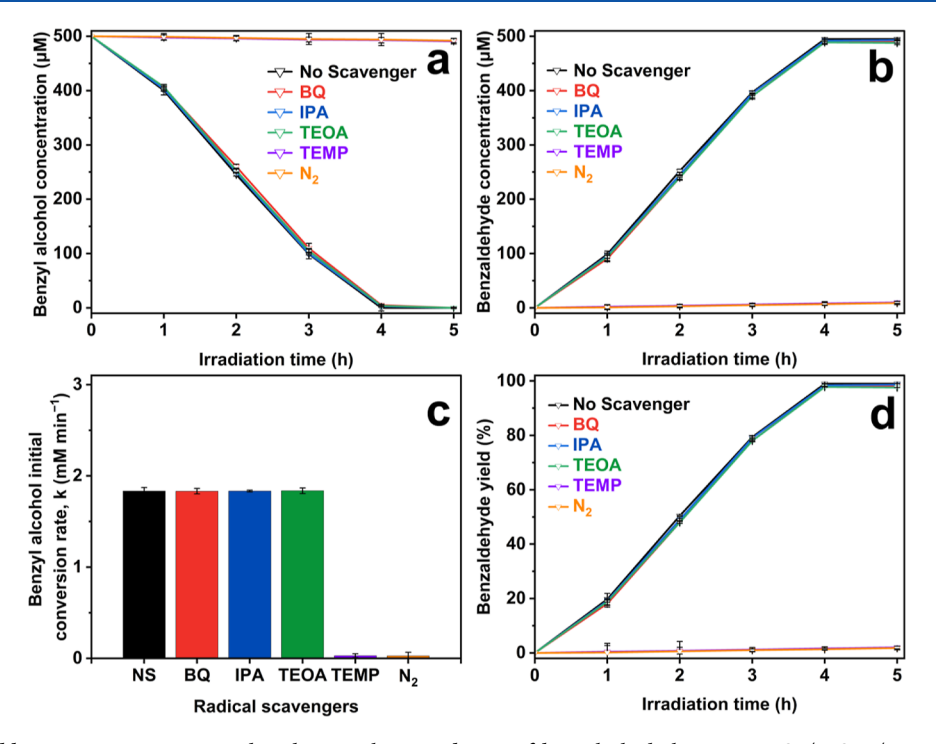


Figure 3. Effect of adding trapping agents on the photocatalytic oxidation of benzyl alcohol using BiVO₄/BiOBr/Au 3%: (a) benzyl alcohol disappearance, (b) benzaldehyde appearance, (c) initial conversion rate of benzyl alcohol, and (d) benzaldehyde yield. Conditions: benzyl alcohol concentration (500 μ M), pH (6.8), photocatalyst weight (30 mg), and temperature (20 °C).

2,2,6,6-tetramethyl piperidine (TEMP) were used to trap superoxide radicals, hydroxyl radicals, holes, and singlet oxygen, respectively. The results (Figure 3) show that the addition of BQ, IPA, and TEOA had no effect on benzyl alcohol conversion or benzaldehyde yield, indicating that neither superoxide radicals, hydroxyl radicals, nor holes were involved in the reaction. On the other hand, the reactivity was completely inhibited upon the addition of TEMP, suggesting that singlet oxygen was a major component in driving the photocatalytic oxidation of benzyl alcohol to benzaldehyde. To identify the source of singlet oxygen, the reaction was conducted using an inert gas, where the reaction vial was purged with N2 for 30 min before starting the reaction, as shown in Figure 3. The data revealed that when the vial was purged with N2, benzyl alcohol conversion and benzaldehyde production were completely inhibited, suggesting that O2 gas was the source for singlet oxygen.

To further confirm the generation of singlet oxygen during the photocatalytic reaction, electron paramagnetic resonance (EPR) analysis was conducted in the presence of TEMP. The sample was prepared by dispersing BiVO₄/BiOBr/Au 3% (1 mg mL⁻¹) in a benzyl alcohol solution (500 μ M) that contained 50 mM TEMP. Next, photogenerated singlet oxygen was produced by irradiating the sample with light in front of a solar simulator for 3 min; then, a sample (50 μ L) was transferred to a capillary tube to be analyzed using EPR, where the generated spectra are shown in Figure 4. The EPR data exhibited a typical spectrum for a TEMP adduct of singlet oxygen with three lines of relative intensities of 1:1:1. These results validate the generation of singlet oxygen within the system, which is responsible for the oxidation of benzyl alcohol to benzaldehyde. In addition, the production of superoxide radicals and hydroxyl radicals was studied using 5-tertbutoxycarbonyl-5-methyl-1-pyrroline-N-oxide (BMPO) as a spin trap; however, no signal was detected, indicating that

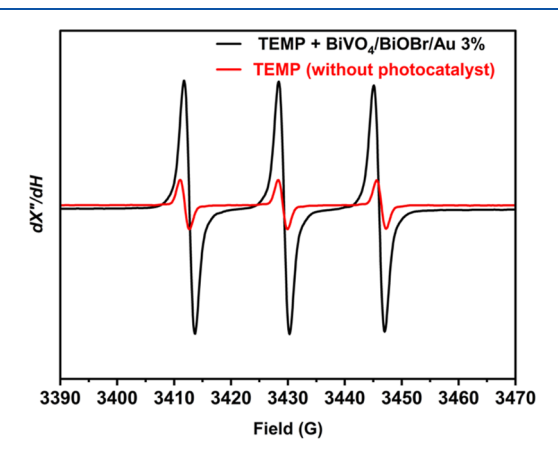


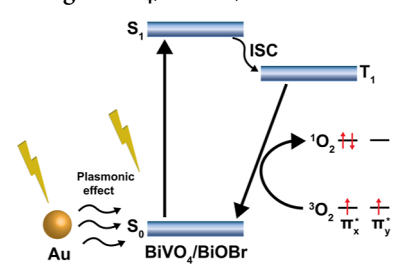
Figure 4. X-band EPR spectra of the TEMP $^{-1}O_2$ adduct in the presence and absence of BiVO $_4$ /BiOBr/Au 3%. Conditions: a microwave power of 10 mW, a frequency of 9.63 GHz, and a temperature of 20 °C.

singlet oxygen is the sole active species produced within the tested system.

Singlet oxygen is a highly reactive species that is typically produced as a result of the oxidation of superoxide radicals via trapped or valence band holes. Harterestingly, our results showed that superoxide radicals have no contribution in the oxidation of benzyl alcohol to benzaldehyde, indicating that the production of singlet oxygen takes place through a completely different process. It has been reported that the spin-flip restriction between the singlet excited state and ground state forbids the conversion of triplet oxygen to singlet oxygen under normal conditions. Gellé et al. Teported that plasmonic nanoparticles can enhance the generation of singlet oxygen via an antenna effect, concentrating the light in the vicinity of the plasmonic nanoparticles. Planas et al. Stated

that hybrid plasmonic nanoparticles enhance the production of $^1\mathrm{O}_2$ by increasing the absorption of light. Macia et al. 52 reported that hybrid silver nanocubes can significantly enhance the production of $^1\mathrm{O}_2$ by exploiting the lightning rod effect, or plasmon hot spots, in the plasmonic nanoparticles. After Au deposition, the extents of benzyl alcohol conversion and benzaldehyde production were significantly enhanced, suggesting that the deposition of plasmonic nanoparticles has remarkably boosted the production of singlet oxygen. Taken together, it is likely that irradiating BiVO₄/BiOBr/Au with light excites the electrons to the singlet state to produce singlet excitons and eventually triplet excitons via intersystem crossing, as shown in Scheme 2. Next, dissolved O₂ reacts with triplet excitons to produce singlet oxygen. 49

Scheme 2. Proposed Mechanism for Singlet Oxygen Production Using BiVO₄/BiOBr/Au 3%



To get further insights about the mechanism of benzyl alcohol oxidation to benzaldehyde, density functional theory calculations were implemented, and the structures of all the reaction components were optimized; the obtained data are presented in Supporting Information, Figure S12. To study whether the oxidation of benzyl alcohol is thermodynamically allowable, the energy barrier and the intrinsic reaction coordinates were estimated (Figure 5). The data showed that singlet oxygen can abstract the hydrogen atoms of the hydroxyl group and alpha carbon by overcoming an energy

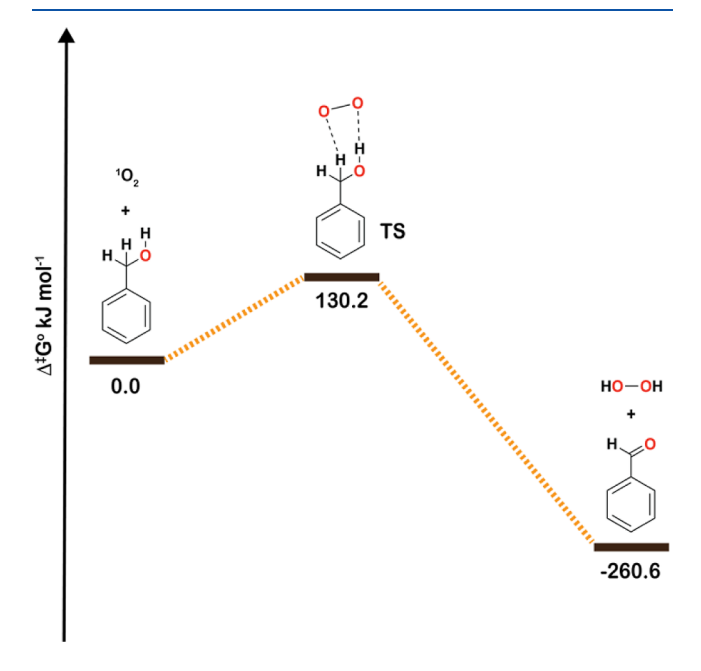


Figure 5. Hydrogen atom abstraction of benzyl alcohol by the $^{1}O_{2}$ energy barrier diagram.

barrier of $130.2 \text{ kJ mol}^{-1}$ to eventually produce benzaldehyde. Moreover, the remarkably negative value obtained for the ΔG during the abstraction of hydrogen atom indicates that the reaction is thermodynamically favored. Theoretically, the abstraction of hydrogen atoms from benzyl alcohol molecules produces benzaldehyde and hydrogen peroxide.

To confirm experimentally the production of hydrogen peroxide during the reaction, aliquots were withdrawn during the reaction and mixed with a TiOSO₄ solution (1.9-2.1%). The mixture was analyzed via UV-vis, as shown in Supporting Information, Figure S13. A broad peak with a λ_{max} of 410 nm was observed, which is ascribed to the yellow titanium peroxide complex (Ti(IV)O22+) that is formed as a result for the reaction of hydrogen peroxide with TiOSO₄ in solution. The results show that the spectrum intensity increases with increasing the reaction time, peaking at 2 h, and that beyond that the spectrum intensity decreases. This increase is ascribed to the production of hydrogen peroxide over the course of the reaction. Interestingly, after 2 h of irradiation, the concentration of hydrogen peroxide declines, which can be attributed to the decomposition of hydrogen peroxide into water and oxygen. Thus, it can be concluded that the photocatalytic oxidation of benzyl alcohol to benzaldehyde produces hydrogen peroxide as a side product, supporting the proposed mechanism.

The recyclability of BiVO₄/BiOBr/Au was tested to assess the sustainability of the proposed system. In this regard, additional experiments were conducted, where BiVO₄/BiOBr/Au 3% was recovered and reused for four consecutive experiments. After each experiment, the recovered BiVO₄/BiOBr/Au 3% was separated, washed, and redispersed in fresh benzyl alcohol solution (500 μ M). After the fourth consecutive experiment (Supporting Information, Figure S14), the benzaldehyde production yield remained almost the same, indicating the ability of the prepared BiVO₄/BiOBr/Au 3% to endure the conditions of the photocatalytic oxidation reaction for at least four runs.

CONCLUSIONS

BiVO₄/BiOBr/Au nanosheets demonstrated outstanding performance in the photocatalytic oxidation of benzyl alcohol to benzaldehyde because of the SPR effect that arises upon decorating BiVO₄/BiOBr with plasmonic gold nanoparticles. Such an improvement expands the light absorption capacity of the semiconducting material to harness visible light irradiation, which eventually fosters the photocatalytic performance. Furthermore, surface plasmons are capable of polarizing the reactants at the metal/liquid interface owing to the dielectric polarization effect, reducing the mass transport limitation at the photocatalyst surface. Our results showed that the superoxide radical has no contribution in the oxidation of benzyl alcohol to benzaldehyde, indicating that the production of singlet oxygen takes place via the intersystem crossing process. In addition, the DFT calculation suggested that singlet oxygen could abstract the hydrogen atoms of the hydroxyl group and alpha carbon to produce benzaldehyde and hydrogen peroxide.

ASSOCIATED CONTENT

Supporting Information

The Supporting Information is available free of charge at https://pubs.acs.org/doi/10.1021/acsanm.3c00293.

XRD pattern of BiVO₄/BiOBr/Au 3%; TEM images of the prepared materials; high-resolution XPS spectra; DRS spectra; N₂ adsorption—desorption isotherms; adsorption of benzyl alcohol; photolysis of benzyl alcohol; photocatalytic oxidation of benzyl alcohol using different DRS spectra, valence band XPS spectra, Mott–Schottky plots, and band structure diagram of BiVO₄ and BiOBr; GC–MS chromatograms; mass spectra; optimized structures; absorbance spectra of titanium peroxide; reusability of BiVO₄/BiOBr/Au 3%; and ICP–OES data for different loadings (PDF)

AUTHOR INFORMATION

Corresponding Author

Leonidas G. Bachas — Department of Chemistry, University of Miami, Coral Gables, Florida 33146, United States; Dr. J.T. Macdonald Foundation Biomedical Nanotechnology Institute, University of Miami, Miami, Florida 33136, United States; orcid.org/0000-0002-3308-6264; Email: bachas@miami.edu

Authors

Ahmed E. ElMetwally — Department of Chemistry, University of Miami, Coral Gables, Florida 33146, United States;

orcid.org/0000-0001-6746-6372

Mostafa Saad Sayed — School of Chemical Engineering, Yeungnam University, Gyeongsan, Gyeongbuk 38541, Republic of Korea

Jae-Jin Shim – School of Chemical Engineering, Yeungnam University, Gyeongsan, Gyeongbuk 38541, Republic of Korea

Marc R. Knecht — Department of Chemistry, University of Miami, Coral Gables, Florida 33146, United States; Dr. J.T. Macdonald Foundation Biomedical Nanotechnology Institute, University of Miami, Miami, Florida 33136, United States; orcid.org/0000-0002-7614-7258

Complete contact information is available at: https://pubs.acs.org/10.1021/acsanm.3c00293

Author Contributions

All authors have given approval to the final version of the manuscript.

Notes

The authors declare no competing financial interest.

ACKNOWLEDGMENTS

Financial support by the University of Miami is gratefully acknowledged. This material is based upon work partially supported by the National Science Foundation under the grant CHE-2203862 (MK).

■ REFERENCES

- (1) Luo, L.; Wang, Z.-j.; Xiang, X.; Yan, D.; Ye, J. Selective Activation of Benzyl Alcohol Coupled with Photoelectrochemical Water Oxidation via a Radical Relay Strategy. *ACS Catal.* **2020**, *10*, 4906–4913.
- (2) Dai, Y.; Ren, P.; Li, Y.; Lv, D.; Shen, Y.; Li, Y.; Niemantsverdriet, H.; Besenbacher, F.; Xiang, H.; Hao, W.; Lock, N.; Wen, X.; Lewis, J. P.; Su, R. Solid Base $\mathrm{Bi}_{24}\mathrm{O}_{31}\mathrm{Br}_{10}(\mathrm{OH})_{\delta}$ with Active Lattice Oxygen for the Efficient Photo-Oxidation of Primary Alcohols to Aldehydes. *Angew. Chem., Int. Ed.* **2019**, *58*, 6265–6270.
- (3) Tojo, G.; Fernández, M. I. Oxidation of Alcohols to Aldehydes and Ketones: A Guide to Current Common Practice; Springer Science & Business Media, 2006.

- (4) Tembe, S. M.; Patrick, G.; Scurrell, M. S. Acetic Acid Production by Selective Oxidation of Ethanol Using Au Catalysts Supported on Various Metal Oxide. *Gold Bull.* **2009**, *42*, 321–327.
- (5) Clarizia, L.; Apuzzo, J.; Di Somma, I.; Marotta, R.; Andreozzi, R. Selective Photo-Oxidation of Ethanol to Acetaldehyde and Acetic acid in Water in Presence of TiO₂ and Cupric Ions Under UV—Simulated Solar Radiation. *Chem. Eng. J.* **2019**, *361*, 1524—1534.
- (6) Xiao, X.; Zheng, C.; Lu, M.; Zhang, L.; Liu, F.; Zuo, X.; Nan, J. Deficient Bi₂₄O₃₁Br₁₀ as a Highly Efficient Photocatalyst for Selective Oxidation of Benzyl Alcohol into Benzaldehyde Under Blue LED Irradiation. *Appl. Catal., B* **2018**, 228, 142–151.
- (7) Xu, C.; Yang, F.; Deng, B.; Zhuang, Y.; Li, D.; Liu, B.; Yang, W.; Li, Y. Ti₃C₂/TiO₂ Nanowires with Excellent Photocatalytic Performance for Selective Oxidation of Aromatic Alcohols to Aldehydes. *J. Catal.* **2020**, 383, 1–12.
- (8) Hu, Y. L.; Fang, D. Efficient and Convenient Oxidation of Alcohols to Aldehydes and Ketones with Molecular Oxygen Mediated by $In(NO_3)_3$ in Ionic Liquid $[C_{12}mim]$ [FeBr₄]. Compt. Rendus Chem. **2015**, 18, 614–618.
- (9) Göksu, H.; Burhan, H.; Mustafov, S. D.; Şen, F. Oxidation of Benzyl Alcohol Compounds in the Presence of CarbonHybrid Supported Platinum Nanoparticles (Pt@CHs) in Oxygen Atmosphere. Sci. Rev. 2020, 10, 5439.
- (10) Zheng, M.; Shi, J.; Yuan, T.; Wang, X. Metal-Free Dehydrogenation of N-Heterocycles by Ternary h-BCN Nanosheets with Visible Light. *Angew. Chem., Int. Ed.* **2018**, *57*, 5487–5491.
- (11) Wang, C.; Astruc, D. Nanogold Plasmonic Photocatalysis for Organic Synthesis and Clean Energy Conversion. *Chem. Soc. Rev.* **2014**, *43*, 7188–7216.
- (12) Zheng, Y.; Gao, T.; Chen, S.; Ferguson, C. T. J.; Zhang, K. A. I.; Fang, F.; Shen, Y.; Khan, N. A.; Wang, L.; Ye, L. CsPbBr₃ Quantum Dots-Decorated Porous Covalent Triazine Frameworks Nanocomposites For Enhanced Solar-Driven H₂O₂ Production. *Compos. Commun.* **2022**, *36*, 101390.
- (13) Zheng, Y.; Ni, X.; Li, K.; Yu, X.; Song, H.; Chen, S.; Khan, N. A.; Wang, D.; Zhang, C. Multi-Heteroatom-Doped Hollow Carbon Nanocages From ZIF-8@CTP Nanocomposites as High-Performance Anodes for Sodium-Ion Batteries. *Compos. Commun.* 2022, 32, 101116.
- (14) Li, R.; Ou, X.; Zhang, L.; Qi, Z.; Wu, X.; Lu, C.; Fan, J.; Lv, K. Photocatalytic Oxidation Of NO on Reduction Type Semiconductor Photocatalysts: Effect of Metallic Bi On Cds Nanorods. *Chem. Commun.* **2021**, *57*, 10067–10070.
- (15) Li, Z.; Huang, W.; Liu, J.; Lv, K.; Li, Q. Embedding CdS@Au into Ultrathin Ti₃–xC₂T_y to Build Dual Schottky Barriers for Photocatalytic H₂ Production. *ACS Catal.* **2021**, *11*, 8510–8520.
- (16) Li, X.; Li, K.; Ding, D.; Yan, J.; Wang, C.; Carabineiro, S. A. C.; Liu, Y.; Lv, K. Effect of Oxygen Vacancies on the Photocatalytic Activity of Flower-Like BiOBr Microspheres Towards NO Oxidation And CO₂ Reduction. *Sep. Purif. Technol.* **2023**, 309, 123054.
- (17) Zheng, B.-F.; Ouyang, T.; Wang, Z.; Long, J.; Chen, Y.; Liu, Z.-Q. Enhanced Plasmon-Driven Photoelectrocatalytic Methanol Oxidation on Au Decorated α -Fe₂O₃ Nanotube Arrays. *Chem. Commun.* **2018**, *54*, 9583–9586.
- (18) Liu, Q.; He, X.; Tao, J.; Tang, H.; Liu, Z.-Q. Oxygen Vacancies Induced Plasmonic Effect for Realizing Broad-Spectrum-Driven Photocatalytic $\rm H_2$ Evolution over an S-Scheme CdS/W $_{18}\rm O_{49}$ Heterojunction. *ChemNanoMat* **2021**, *7*, 44–49.
- (19) Huang, S.; Feng, F.; Huang, R.-T.; Ouyang, T.; Liu, J.; Liu, Z.-Q. Activating C—H Bonds by Tuning Fe Sites and an Interfacial Effect for Enhanced Methanol Oxidation. *Adv. Mater.* **2022**, *34*, 2208438.
- (20) Higashimoto, S.; Kitao, N.; Yoshida, N.; Sakura, T.; Azuma, M.; Ohue, H.; Sakata, Y. Selective Photocatalytic Oxidation of Benzyl Alcohol and its Derivatives into Corresponding Aldehydes by Molecular Oxygen on Titanium Dioxide Under Visible Light Irradiation. *J. Catal.* **2009**, *266*, 279–285.
- (21) Su, F.; Mathew, S. C.; Lipner, G.; Fu, X.; Antonietti, M.; Blechert, S.; Wang, X. mpg-C₃N₄-Catalyzed Selective Oxidation of

- Alcohols Using O_2 and Visible Light. J. Am. Chem. Soc. 2010, 132, 16299–16301.
- (22) Liu, Y.; Zhang, P.; Tian, B.; Zhang, J. Core-Shell Structural CdS@SnO₂ Nanorods with Excellent Visible-Light Photocatalytic Activity for the Selective Oxidation of Benzyl Alcohol to Benzaldehyde. ACS Appl. Mater. Interfaces 2015, 7, 13849–13858.
- (23) Wan, J.; Du, X.; Liu, E.; Hu, Y.; Fan, J.; Hu, X. Z-Scheme Visible-Light-Driven Ag₃PO₄ nanoparticle@MoS₂ Quantum Dot/Few-Layered MoS₂ Nanosheet Heterostructures with High Efficiency and Stability for Photocatalytic Selective Oxidation. *J. Catal.* **2017**, 345, 281–294.
- (24) Zhang, B.; Li, J.; Gao, Y.; Chong, R.; Wang, Z.; Guo, L.; Zhang, X.; Li, C. To Boost Photocatalytic Activity in Selective Oxidation of Alcohols on Ultrathin $\mathrm{Bi}_2\mathrm{MoO}_6$ Nanoplates with Pt Nanoparticles as Cocatalyst. *J. Catal.* **2017**, 345, 96–103.
- (25) Li, H.; Qin, F.; Yang, Z.; Cui, X.; Wang, J.; Zhang, L. New Reaction Pathway Induced by Plasmon for Selective Benzyl Alcohol Oxidation on BiOCl Possessing Oxygen Vacancies. *J. Am. Chem. Soc.* **2017**, *139*, 3513–3521.
- (26) Rather, R. A.; Mehta, A.; Lu, Y.; Valant, M.; Fang, M.; Liu, W. Influence of Exposed Facets, Morphology and Hetero-Interfaces of BiVO₄ on Photocatalytic Water Oxidation: A review. *Int. J. Hydrogen Energy* **2021**, *46*, 21866–21888.
- (27) Xie, M.; Zhang, Z.; Han, W.; Cheng, X.; Li, X.; Xie, E. Efficient Hydrogen Evolution Under Visible Light Irradiation over $BiVO_4$ Quantum Dot Decorated Screw-Like SnO_2 Nanostructures. *J. Mater. Chem. A* **2017**, *5*, 10338–10346.
- (28) Grigioni, I.; Abdellah, M.; Corti, A.; Dozzi, M. V.; Hammarström, L.; Selli, E. Photoinduced Charge-Transfer Dynamics in WO₃/BiVO₄ Photoanodes Probed through Midinfrared Transient Absorption Spectroscopy. *J. Am. Chem. Soc.* **2018**, *140*, 14042–14045.
- (29) Liu, S.; Pan, J.; Li, X.; Meng, X.; Yuan, H.; Li, Y.; Zhao, Y.; Wang, D.; Ma, J.; Zhu, S.; Kong, L. In Situ Modification of BiVO₄ Nanosheets on Graphene for Boosting Photocatalytic Water Oxidation. *Nanoscale* **2020**, *12*, 14853–14862.
- (30) Li, W.; Zhang, Y.; Bu, Y.; Chen, Z. One-Pot Synthesis of the BiVO₄/BiOBr Heterojunction Composite for Enhanced Photocatalytic Performance. *J. Alloys Compd.* **2016**, *680*, *677*–*684*.
- (31) Olagunju, M. O.; Zahran, E. M.; Reed, J. M.; Zeynaloo, E.; Shukla, D.; Cohn, J. L.; Surnar, B.; Dhar, S.; Bachas, L. G.; Knecht, M. R. Halide Effects in BiVO₄/BiOX Heterostructures Decorated with Pd Nanoparticles for Photocatalytic Degradation of Rhodamine B as a Model Organic Pollutant. *ACS Appl. Nano Mater.* **2021**, *4*, 3262–3272.
- (32) Wang, D.; Pillai, S. C.; Ho, S.-H.; Zeng, J.; Li, Y.; Dionysiou, D. D. Plasmonic-Based Nanomaterials for Environmental Remediation. *Appl. Catal., B* **2018**, 237, 721–741.
- (33) Li, Z.; Meng, X. Recent Development on Palladium Enhanced Photocatalytic Activity: A review. J. Alloys Compd. 2020, 830, 154669.
- (34) Zhang, X.; Chen, Y. L.; Liu, R.-S.; Tsai, D. P. Plasmonic photocatalysis. *Rep. Prog. Phys.* **2013**, *76*, 046401.
- (35) Tian, Z.; Wu, S.; Wang, P.; Cai, Y.; Liang, D.; Ye, Y.; Liu, J.; Liang, C. Aqueous Dispersed Ablated Bismuth Species and their Potential as Colloidal Bi Precursors in Synthetic Strategies. CrystEngComm 2015, 17, 3015–3022.
- (36) Arumugasamy, S. K.; Govindaraju, S.; Yun, K. Manganese Ions Conjugated on Layered Bismuth Oxyhalides for High-Performance Pseudocapacitors and Efficient Oxygen Evolution Catalysts. *Inorg. Chem. Front.* **2020**, *7*, 4412–4423.
- (37) Ngo, T. T.; Lozano, G.; Míguez, H. Enhanced Up-Conversion Photoluminescence in Fluoride—Oxyfluoride Nanophosphor Films by Embedding Gold Nanoparticles. *Mater. Adv.* **2022**, *3*, 4235–4242.
- (38) ElMetwally, A. E.; Sayed, M. S.; Zeynaloo, E.; Zahran, E. M.; Shim, J.-J.; Knecht, M. R.; Bachas, L. G. Hierarchical Core—Shell ACOF-1@BiOBr as an Efficient Photocatalyst for the Degradation of Emerging Organic Contaminants. *J. Phys. Chem. C* **2022**, *126*, 2503—2516
- (39) Liu, C.; Mao, S.; Shi, M.; Hong, X.; Wang, D.; Wang, F.; Xia, M.; Chen, Q. Enhanced Photocatalytic Degradation Performance of

- BiVO₄/BiOBr through Combining Fermi Level Alteration and Oxygen Defect Engineering. *Chem. Eng. J.* **2022**, 449, 137757.
- (40) Li, Y.; Liao, D.; Li, T.; Zhong, W.; Wang, X.; Hong, X.; Yu, H. Plasmonic Z-Scheme Pt-Au/BiVO₄ Photocatalyst: Synergistic Effect of Crystal-Facet Engineering and Selective Loading of Pt-Au Cocatalyst for Improved Photocatalytic Performance. *J. Colloid Interface Sci.* **2020**, 570, 232–241.
- (41) Jenkins, J. A.; Zhou, Y.; Thota, S.; Tian, X.; Zhao, X.; Zou, S.; Zhao, J. Blue-Shifted Narrow Localized Surface Plasmon Resonance from Dipole Coupling in Gold Nanoparticle Random Arrays. *J. Phys. Chem. C* **2014**, *118*, 26276–26283.
- (42) Gwo, S.; Chen, H.-Y.; Lin, M.-H.; Sun, L.; Li, X. Nanomanipulation and Controlled Self-Assembly of Metal Nanoparticles and Nanocrystals for Plasmonics. *Chem. Soc. Rev.* **2016**, *45*, 5672–5716
- (43) Schünemann, S.; van Gastel, M.; Tüysüz, H. A CsPbBr₃/TiO₂ Composite for Visible-Light-Driven Photocatalytic Benzyl Alcohol Oxidation. *ChemSusChem* **2018**, *11*, 2057–2061.
- (44) Shen, M.; Shi, Y.; Wang, Z.; Wu, T.; Hu, L.; Wu, L. Enhanced Photocatalytic Benzyl Alcohol Oxidation over Bi₄Ti₃O₁₂ Ultrathin Nanosheets. *J. Colloid Interface Sci.* **2022**, *608*, 2529–2538.
- (45) Zou, J.; Wang, Z.; Guo, W.; Guo, B.; Yu, Y.; Wu, L. Photocatalytic Selective Oxidation of Benzyl Alcohol over ZnTi-LDH: The Effect of Surface OH groups. *Appl. Catal., B* **2020**, *260*, 118185.
- (46) Xing, F.; Zeng, R.; Cheng, C.; Liu, Q.; Huang, C. POM-Incorporated ZnIn₂S₄ Z-Scheme Dual-Functional Photocatalysts for Cooperative Benzyl Alcohol Oxidation and H₂ Evolution in Aqueous Solution. *Appl. Catal., B* **2022**, *306*, 121087.
- (47) Giannakoudakis, D. A.; Qayyum, A.; Barczak, M.; Colmenares-Quintero, R. F.; Borowski, P.; Triantafyllidis, K.; Colmenares, J. C. Mechanistic and Kinetic Studies of Benzyl Alcohol Photocatalytic Oxidation by Nanostructured Titanium (Hydro)oxides: Do We Know the Entire Story? *Appl. Catal., B* **2023**, 320, 121939.
- (48) Nosaka, Y.; Nosaka, A. Y. Generation and Detection of Reactive Oxygen Species in Photocatalysis. *Chem. Rev.* **2017**, *117*, 11302–11336.
- (49) Wang, H.; Jiang, S.; Chen, S.; Li, D.; Zhang, X.; Shao, W.; Sun, X.; Xie, J.; Zhao, Z.; Zhang, Q.; Tian, Y.; Xie, Y. Enhanced Singlet Oxygen Generation in Oxidized Graphitic Carbon Nitride for Organic Synthesis. *Adv. Mater.* **2016**, *28*, 6940–6945.
- (50) Gellé, A.; Price, G. D.; Voisard, F.; Brodusch, N.; Gauvin, R.; Amara, Z.; Moores, A. Enhancing Singlet Oxygen Photocatalysis with Plasmonic Nanoparticles. *ACS Appl. Mater. Interfaces* **2021**, *13*, 35606–35616.
- (51) Planas, O.; Macia, N.; Agut, M.; Nonell, S.; Heyne, B. Distance-Dependent Plasmon-Enhanced Singlet Oxygen Production and Emission for Bacterial Inactivation. *J. Am. Chem. Soc.* **2016**, *138*, 2762–2768.
- (52) Macia, N.; Bresoli-Obach, R.; Nonell, S.; Heyne, B. Hybrid Silver Nanocubes for Improved Plasmon-Enhanced Singlet Oxygen Production and Inactivation of Bacteria. *J. Am. Chem. Soc.* **2019**, *141*, 684–692.